

On the Runway Cascade of Transformers for Language Modeling

Hunjae Lee¹ Corey Clark¹

Abstract

In decoder-only (causal) transformers, the computation graph created by causal masking routes information through both direct-path attention and indirect paths formed by intermediate tokens. We denote these indirect paths between token pairs as their *runways*. We argue that certain failure modes of causal transformers as observed by a growing body of recent works are likely exacerbated by a misalignment between these two information propagation modes. We formalize *runway cascade* as a phenomenon whereby this misalignment results in redundancies and irrelevant information cascading to token representations despite adequately learned attention patterns. As a solution, we propose *runway-aware rewiring* as a more explicit way of incorporating runway context directly into each token’s direct-path attention. This mechanism re-wires the attention pattern for each token based on a summary of its runway landscape, enabling awareness of accumulating representational influences and allowing for more balanced information propagation. Our proposed methodology introduces no additional parameters and can seamlessly be integrated into standard attention mechanism. Empirically, our rewired transformer results in steady improvements in general language modeling as well as noticeably stronger information retrieval and extrapolation abilities compared to standard transformers.

1. Introduction

Causal, decoder-only, transformers make up a majority of modern LLM architectures (Achiam et al., 2023; Comanici et al., 2025). Despite their tremendous success, they have been observed to exhibit failure points and unexpected phenomena. Some of these instances include lost-in-the-middle phenomenon (Liu et al., 2024) on retrieval tasks, last-token

representation collapse (Barbero et al., 2024), the emergence of position bias favoring early positions in the sequence (Wu et al., 2025), and the development of attention sinks (Xiao et al., 2024; Gu et al., 2025). Viewing transformers as an instance of graph neural networks (GNNs) (Joshi, 2025), many of these phenomena can be contextualized through information propagation theory of GNNs, a field with a rich literature studying representational and topological bottlenecks. Namely, theory of over-squashing and over-smoothing in GNNs have been instrumental in fostering a unified perspective on these seemingly disconnected failure modes of transformers (Wu et al., 2024; Barbero et al., 2024; Arroyo et al., 2025).

At the heart of these failure modes lie the computation graph structure created by causal masking in decoder-only transformers. This causal graph has been shown to create position bias that, when taken to the limit, make early tokens in the sequence dominate the representation landscape (Wu et al., 2025; Barbero et al., 2025a). Likewise, the causal graph structure is also responsible for creating last-token representation collapse, whereby certain distinct sequences become arbitrarily similar in their last token representation (Barbero et al., 2024).

In causal attention, tokens influence subsequent positions in two ways: (1) through direct connections and (2) indirectly by influencing intermediate tokens along the *runway*. We define the runway of two tokens as the collection of indirect paths between them made up of intermediate tokens. To study their influence on information propagation, we formulate a GNN-theory style bound for causal transformers and show that their representational sensitivity is controlled by the given destination token’s own attention pattern (direct influence) acting as a gate, composing the mixture of accumulated attention patterns along its runway (indirect influences). Building on top of the effects of position bias studied by recent works (Barbero et al., 2025a; Wu et al., 2025), we argue that a misalignment between these direct and indirect representational influences can exacerbate information propagation issues in causal transformers.

In this work, we introduce *runway cascade* as a phenomenon whereby direct-path attention no longer adequately controls the indirect influences and thereby resulting in cascade of redundancies and irrelevant information on token represen-

¹Department of Computer Science, Southern Methodist University, Dallas TX USA. Correspondence to: Hunjae Lee <hunjael@smu.edu>.

tations. We argue that this stems from standard attention mechanism remaining unaware of accumulating runway influences and show that it can occur even when the attention patterns are adequately learned. As such, we propose a more explicit way of incorporating runway context directly into row-wise attention calculation. We introduce a runway-aware rewiring technique that re-wires the attention pattern for each token based on a computed *runway-coefficient*. This allows each token’s attention pattern to discern accumulated representational influences along the runway and to re-weight the attention scores accordingly for more balanced information propagation. Our proposed solution introduces no additional parameters and can be seamlessly integrated with standard attention.

2. Background and Related Works

2.1. Interpreting Causal Transformers as a GNN

In order to study transformers in part through the lens of GNN theory, we first make the connection that transformers can be seen as an instance of GNNs (Joshi, 2025). Extending from (Joshi, 2025) which constrained its analysis to fully-connected, non-causal attention, we interpret causal transformers as an attention-based message-passing GNN as:

$$h_i^{(l+1)} = \phi \left(h_i^{(l)}, \sum_{j \leq i} A_{ij} \psi(h_i^{(l)}, h_j^{(l)}) \right) \quad (1)$$

where the aggregate function ψ represents the attention-based weighted sum of tokens dictated by lower-triangular and row-stochastic adjacency operator A as:

$$\psi(h_i^{(l)}, h_j^{(l)}) = h_j^{(l)} W_V \quad (2)$$

$$A_{ij} = \text{SoftMax}(h_i^{(l)} W_Q \cdot h_j^{(l)} W_K) \quad (3)$$

and the update function ϕ represents intra-token evolution to the next layer as follows:

$$\phi(h_i^{(l)}, \bar{h}_i^{(l)}) = \text{MLP}(h_i^{(l)} + \bar{h}_i^{(l)}) \quad (4)$$

$$\bar{h}_i^{(l)} = \sum_{j \leq i} A_{ij} \psi(h_i^{(l)}, h_j^{(l)}) \quad (5)$$

By interpreting causal transformers as an instance of a message-passing GNN, information propagation patterns in causal transformers can be studied under a more graph-theoretic lens.

2.2. Information Propagation Theory

Analyzing failure modes and unexpected phenomena of transformer-based language models through the lens of information propagation theory is a recent but increasingly favored approach. In particular, theory of over-squashing in GNNs has been helpful in understanding related issues in transformers.

Over-squashing in GNNs. Over-squashing (Alon & Yahav, 2021; Topping et al., 2022; Di Giovanni et al., 2023) is a phenomenon in GNNs where exponentially growing receptive field of nodes result in over-compression of information into fixed-sized node representations, inevitably causing distortion or even loss of certain information. This has been observed as a consequence of long-range information propagation (Alon & Yahav, 2021) but also of graph topology (Topping et al., 2022; Black et al., 2023; Giovanni et al., 2024). In particular, (Giovanni et al., 2024) interprets over-squashing as a result of misalignment between the graph topology and the task at hand. Many issues of transformers arising from the causal graph can be interpreted under this framework, where the causal graph creates misalignment between its topology and the task at hand despite being a practical tool for handling next-token prediction schemes. Over-squashing in GNNs is known as representation collapse¹ in transformers, a phenomenon that has been shown to disproportionately affect the last token in the sequence (Barbero et al., 2024).

Graph Rewiring. A well-studied methodology to alleviate information propagation issues and to better align the graph topology to the task at hand is graph rewiring. There’s broadly two different objectives: spatial rewiring (Abboud et al., 2022; Brüel-Gabrielsson et al., 2022), and spectral rewiring (Karhadkar et al., 2023; Jamadandi et al., 2024). Many works also optimize for more specific quantities, such as effective resistance (Black et al., 2023), commute time (Giovanni et al., 2024; Sterner et al., 2024), and the spectral gap of the graph Laplacian (Deac et al., 2022; Wilson et al., 2024).

Graph rewiring approaches have also been applied to transformers. For the most part, they rewire the computation graph for sparsity and computational efficiency (Shirzad et al., 2023; 2024) and not for topological improvements. Under this interpretation, sparse transformers (Beltagy et al., 2020; Zaheer et al., 2020) in general can be seen as ways of rewiring the attention pattern to achieve computational efficiency.

A majority of graph rewiring approaches (including aforementioned works) opt for *hard-rewiring*, whereby edges are

¹We use over-squashing and representation collapse interchangeably in our work

added or deleted to change the connectivity of the graph in a binary manner. In our proposed methodology, however, we opt for a *soft-rewiring* approach, changing attention patterns based on the rewiring criteria without changing the graph topology itself. We do this to maintain causality and to make the comparison against standard causal transformers as one-to-one as possible.

2.3. Position Bias and Information Propagation Issues in Transformers

While being a practical and effective solution for enforcing causality, the application of causal masking in the shape of an upper-triangular mask creates interesting, and potentially unexpected phenomena for transformers in practice. Namely, the causal graph of the transformer, now directed and bipartite, creates a position bias that favors early positions (Wu et al., 2025). Intuitively, the earlier the position in the sequence, the more future tokens attend back to it, giving it more opportunities to influence other tokens to preserve and refine its own information. This has practical consequences, with works showing asymmetric performance degradation based on position dependencies or order of examples (Lu et al., 2022; Hou et al., 2024; Fang et al., 2025). Position bias is also related to the emergence of attention sinks (Xiao et al., 2024; Gu et al., 2025; Barbero et al., 2025a), a phenomenon where the first few tokens of the sequence get disproportionately high attention weights. In addition, position bias of causal transformers can induce over-squashing or representation collapse of the last token in certain distinct sequences, as illustrated by (Barbero et al., 2024).

While some recent works have begun relating these emergent properties of causal graphs in transformers, they typically focus on their influence on absolute positions in the sequence. For example, (Wu et al., 2025; Barbero et al., 2025a) focus on the role of the early positions in the sequence while (Barbero et al., 2024) studies the effects of the causal graph on the final token in the sequence. As such, a generalized understanding on how relative distances between arbitrary token pairs affect information propagation has not been made explicit. Likewise, practical solutions that address these information propagation issues created by the geometry of the causal graph remain limited.

On Positional Encodings. The study of position bias is related, but distinct, from the study of positional encodings (PEs) (Kazemnejad et al., 2023; Su et al., 2024; Barbero et al., 2025b). Intuitively, while PEs are a study of how order is represented in attention mechanisms, position bias is a study of how the given architecture processes order. The latter reveals emergent topological bottlenecks hindering information propagation, and how they can override inductive biases meant to be provided by the former.

3. Runway Cascade

3.1. Information Flow in Transformers

In causal attention, information from a given source token h_s flows to its destination token h_d in two ways (for arbitrary source and destination tokens $s \leq d$ in the sequence). First, *direct connections* allow h_s to reach h_d directly in one-hop connection. The strength of such direct connection is controlled by the destination token's own row-wise attention pattern. Second, *indirect connections* between h_s and h_d allow h_s to influence intermediate tokens h_j (where $s < j < d$) to propagate its own information along the indirect paths to h_d . We denote the collection of all indirect paths between h_s and h_d as their *runway*.

Definition 3.1 (Runway). Let $\mathcal{G} = (V, E)$ be a directed, bipartite graph where V denotes vertices (nodes) and E denotes edges. A path from nodes s and d is a vertex sequence $p = (v_0, \dots, v_l)$ with $v_0 = s$ and $v_l = d$, s.t. $(v_{i-1}, v_i) \in E$ for all i and distinct vertices. An indirect path is any path where the path length $l \geq 2$, or equivalently if the internal vertex set $\{v_1, \dots, v_{l-1}\} \neq \emptyset$. Let $P_{\mathcal{G}}(s, d)$ be the set of all paths between s and d . Then, the runway of nodes s and d is defined as the set \mathcal{R}_{ds} where:

$$\mathcal{R}_{ds} = \{(v_0, \dots, v_l) \in P_{\mathcal{G}}(s, d) : l \geq 2\}$$

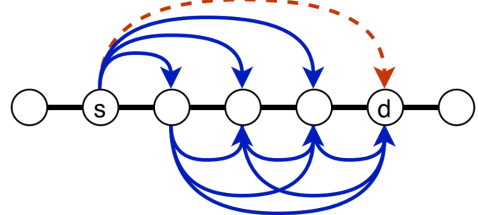


Figure 1. Visualizing two types of paths between token s and d along the causal graph: (1) direct path (in dotted red) and (2) indirect paths (in solid blue).

Figure 1 illustrates the runway \mathcal{R}_{ds} of tokens h_s and h_d in solid blue paths while denoting the direct path in dotted red. While information of token h_s has many paths flowing into h_d (red + blue paths), only its direct path (in dotted red) is controlled explicitly by h_d with respect to h_s in isolation. On the other hand, accumulated information of h_s in the runway (propagated along solid blue paths) are absorbed into intermediate tokens. While these intermediate tokens ultimately influence h_d 's representation through their own direct connections, h_d can only attend to them without being able to isolate the contribution of h_s . In addition, though the intermediate tokens do have some control over whether to absorb information from h_s or not in their direct connections to h_s , the continuous nature of the softmax function in the attention mechanism prevents them from ignoring h_s entirely (Wu et al., 2023; 2025).

Lemma 3.2 (Lemma 2 from Wu et al. (2023)). *Assume that the attention function is continuous and the point-wise nonlinear activation function $\sigma(\cdot)$ satisfies $0 \leq \frac{\sigma(x)}{x} \leq 1$ for $x \neq 0$ and $\sigma(0) = 0$. Then, there exists $\epsilon > 0$ s.t. for all $t \in \mathbb{N}_{\geq 0}$ and for any $(i, j) \in E$, we have $a_{ij}^{(t)} > \epsilon$.*

Lemma 3.2 states that attention mechanism cannot disconnect any valid edge between nodes/tokens given the continuous nature of the softmax function and that each edge (i, j) must be assigned a non-zero attention weight $a_{ij}^{(t)} > \epsilon$, $\epsilon > 0$. This means that information of h_s accumulates *inevitably* along the runway to h_d . Position bias exacerbates this effect, giving h_s more opportunities to preserve and refine its information the earlier its position in the sequence. Because the only path through which h_d can control h_s in isolation is through its direct path, it has no explicit control over how much of h_s flows to h_d along the runway through intermediate tokens. As discussed in subsequent sections, we argue that a *misalignment* between direct-path attention and runway accumulated information can result in redundant or semantically irrelevant information to cascade to tokens even if the attention pattern is adequately learned.

3.2. Runway Induced Representation Bottlenecks

The effects of the runway in causal graphs as discussed in Section 3.1 can be formalized using the Jacobian of node/token representations. The Jacobian of node representations is a measure of its sensitivity with respect to a given node, and is often used in GNN literature to upper-bound and analyze representation bottlenecks and over-squashing effects.

Theorem 3.3. *Assume a source token h_s at layer $L \geq 0$ and destination token h_d at $r \geq 0$ layers apart and on arbitrary positions $s \leq d$. In addition, let $C > 0$ be some constant and A be lower-triangular, row-stochastic adjacency operator. Then, the representational sensitivity of h_d with respect to h_s can be bounded as:*

$$\left\| \frac{\partial h_d^{(L+r)}}{\partial h_s^{(L)}} \right\| \leq C^r \left(\prod_{t=0}^{r-1} (I + A^{(L+t)}) \right)_{ds}$$

The full theorem and its proof are provided in the Appendix (Section A.1).

Theorem 3.3 states that representation sensitivity of token h_d with respect to h_s can be upper-bounded by the accumulation of attention patterns A_{ds} between h_d and h_s across layers with the residual stream I reinforcing self-representations. This is similar to findings from Theorem 5.1 (Barbero et al., 2024) with some key distinctions for interpretive and generalization purposes. Namely, our findings are both position and layer agnostic and describes representation sensitivities of tokens at arbitrary positions at arbitrary layers. This is in contrast to Theorem 5.1 in (Barbero et al.,

2024) which only studied over-squashing effects of the final token in the sequence at the final layer with respect to tokens at the input layer. While these are largely generalization improvements, our Theorem 3.3 does indicate that runway influences impact representation learning throughout the sequence of tokens across layers, not just the final token at the final layer.

This also suggests that tokens in the middle of the sequence may be most susceptible to being used as information propagators. The longer the sequential distance between source and destination tokens, the longer their runway and the more intermediate tokens (towards the middle of the sequence) get involved. This may lead to tokens toward the middle of the sequence being *over-used* as runways for various token pairs at either ends of the sequence, perhaps even at the cost of losing their own representation sharpness. This aligns well with the observed lost-in-the-middle effects (Liu et al., 2024) where performance tends to degrade in retrieval tasks (where representation sharpness is particularly important) towards the middle of the sequence and show a U-shaped performance curve (Barbero et al., 2024).

In addition, Theorem 3.3 is constructed such that the contribution of the direct path can be separated from the accumulating influence of the runway. Namely, the RHS of Theorem 3.3 can be expanded as:

$$\begin{aligned} \left\| \frac{\partial h_d^{(L+r)}}{\partial h_s^{(L)}} \right\| \leq & C^{r+1} \left(\left(\prod_{t=0}^{r-2} (I + A^{(L+t)}) \right)_{ds} \right. \\ & \left. + \sum_{w \in \mathcal{N}(d)} A_{dw}^{(L+r-1)} \left(\prod_{t=0}^{r-2} (I + A^{(L+t)}) \right)_{ws} \right) \end{aligned} \quad (6)$$

where the first term inside the main parenthesis $\left(\prod_{t=0}^{r-1} (I + A^{(L+t)}) \right)_{ds}$ is the self-token update term $\partial \phi_1$ and the second term shows the structure of cross-token mixing, isolated as:

$$\sum_{w \in \mathcal{N}(d)} A_{dw}^{(L+r-1)} \left(\prod_{t=0}^{r-2} (I + A^{(L+t)}) \right)_{ws} \quad (7)$$

Here, $A_{dw}^{(L+r-1)}$ denotes the direct-path attention pattern for h_d (over its immediate neighbors $w \in \mathcal{N}(d)$) and $\left(\prod_{t=0}^{r-2} (I + A^{(L+t)}) \right)_{ws}$ denotes the accumulating influence of the runway. This shows that the destination token's own attention pattern (over its row) acts as a gate that chooses a mixture of indirectly propagated information along its runway. However, A_{dw} is only conditioned on the individual neighbor tokens h_w , $\forall w \in \mathcal{N}(d)$ without explicit access to the global landscape of the runway,

which can lead to A_{dw} being unaware of global cascade of redundant or semantically uninformative information.

Lemma 3.4 (Blindspots for standard attention mechanism). *Let token representation $h_w = \tilde{h}_w + \delta$ where \tilde{h}_w is (unique) token representation that differentiates h_w and δ denotes the runway influences on h_w . Assume also that δ can be further decomposed into $\delta = \delta_c + \delta_r$ where δ_c is the row-wise perturbation (common mode influence) and δ_r is the residual deviation from row-wise perturbation. Then, attention weights cannot discern runway influences except through (small) residual deviations as:*

$$\|a_d - \tilde{a}_d\| \leq \sigma_0 P \|\delta_r\|$$

Here, σ_0 represents the global Lipschitz constant and P represents the bound on model terms. Full lemma and its proof are provided in Section A.2.

Lemma 3.4 states that when runway influences largely carry common mode information (i.e. shared information between tokens), the attention weights increasingly become insensitive toward such global influences. Viewing attention mechanism as a contractive mixing operation whose repeated application drives representations closer together (Wu et al., 2023; Barbero et al., 2025a; Arroyo et al., 2025), these common mode influences may grow larger with model depth. In addition, these common mode influences are invariant to attention aggregation and cascade forward in attention mechanism.

Theorem 3.5 (Runway Cascade). *Let token representation $h_w = \tilde{h}_w + \delta$ where \tilde{h}_w is (unique) token representation that differentiates h_w and δ denotes the runway influences on h_w . Assume also that δ can be further decomposed into $\delta = \delta_c + \delta_r$ where δ_c is the row-wise perturbation (common mode influence) and δ_r is the residual deviation from row-wise perturbation. Then, their common mode runway influence must persist and cascade forward in the attention mechanism.*

The full theorem and its proof are provided in Section A.2.

The implication of runway cascade is that redundant and irrelevant information can have a snowballing effect where the more they influence the global runway landscape, the more they become invisible to the attention mechanism and cascade forward, creating more influence. This suggests that information propagation in causal transformers may be improved if the attention mechanism is explicitly conditioned on runway influences. With this insight, we introduce a runway-aware rewiring strategy for the causal graph.

4. Runway Aware Rewiring

With the observation that direct attention patterns in their standard formulation may be inadequate in accounting for

runway effects, we introduce a runway-aware rewiring strategy for causal attention. Instead of simply computing attention on individual neighbor tokens where common mode redundancies may carry forward unnoticed, we contextualize each token against a global runway summary and rewire their attention pattern accordingly. Our rewiring is a soft-rewiring approach that scales each edge in the causal graph with computed runway-coefficients.

At the core of our rewiring strategy is quantifying how much of a given token h_m in the runway \mathcal{R}_{ds} already carries runway-accumulated redundancies with respect to the destination token h_d where $s \leq m < d - 1$. We denote this quantity as *runway-coefficient* r_{dm} which is calculated as follows:

$$r_{dm} = \sigma(\tau(h_{d-1}, h_m)) \quad (8)$$

where given h_d , the token that immediately precedes it in the sequence h_{d-1} computes a compatibility score against each h_m for all $m, s \leq m < d - 1$ to evaluate how much of the runway is already dominated by h_m through indirect paths. Intuitively, if h_{d-1} is highly compatible with h_m , then this indicates that h_m is sufficiently represented in the runway via indirect paths already and thus its contribution should be scaled down proportionally for h_d . In this way, the past-adjacent token h_{d-1} serves as a global summary of the runway for h_d , giving context for each h_m to measure against. We choose h_{d-1} because it represents the most up-to-date summary of the runway for each h_d , making it an appropriate measure of runway landscape. The raw compatibility measure $\tau(\cdot)$ can be calculated with a dot-product (Equation (9)) to keep it parameter-free or with a bilinear form (Equation (10)) to inject some learnability:

$$\tau_{\text{dot}}(h_{d-1}, h_m) = h_{d-1}^T \cdot h_m \quad (9)$$

$$\tau_{\text{bilinear}}(h_{d-1}, h_m) = h_{d-1}^T B h_m, B \in \mathbb{R}^{N \times N} \quad (10)$$

We use the dot-product formulation (Equation (9)) in our main experiments to make sure our rewired model introduces no additional parameters for fair comparison against the standard transformer. We do perform ablations with the bilinear form (Equation (10)) in Section C.4 and find that it is comparable in performance to the dot-product approach.

Finally, a smooth thresholding function like sigmoid is applied as $\sigma(\cdot)$ to ensure $0 < r_{dm} < 1$.

As large r_{dm} indicates sufficient representation of h_m in the runway, the direct-path attention between h_d and h_m should then be scaled down proportionally. The multiplicative scaling is done using the complement $\bar{r}_{dm} = 1 - r_{dm}$ to

ensure larger runway-coefficient leads to stronger down-scaling. Namely, given the original edge-weights of the causal transformer:

$$e_{dm} = \text{SoftMax}_{\mathcal{N}(d)}\left(\frac{(h_d W_Q)^T \cdot (h_m W_K)}{\sqrt{d_k}}\right) \quad (11)$$

the edge weights are scaled (Equation (12)) and re-normalized (Equation (13)) to ensure each row sums up to 1.0 as:

$$\tilde{e}_{dm} = e_{dm} \cdot \bar{r}_{dm} \quad (12)$$

$$\hat{e}_d = \frac{\tilde{e}_d}{\sum_m \tilde{e}_{dm}} \quad (13)$$

Finally, the complete mechanism for runway-aware rewiring for h_d can be expressed as:

$$h_d^{(l+1)} = \sum_m \hat{e}_{dm}^{(l)} (h_m^{(l)} W_V) \quad (14)$$

Due to the reliance on the immediate preceding token h_{d-1} for compatibility calculations, they are never scaled down for h_d , forming a directed line-graph like topology among tokens wherein information propagates without re-wiring. Likewise, each token’s self connection is also preserved without down-scaling. In our setup, edges are always down-scaled and never boosted by runway coefficients. However, due to re-normalization and the mechanics of softmax, edges with relatively small down-scaling effects end up getting boosted overall relative to edges with more severe down-scaling. This way, our rewiring can not only dampen unnecessarily dominant signals but it can also boost over-squashed signals later on to re-introduce them into the representation landscape if need be.

In implementation, our rewiring strategy re-purposes the value vectors from one of the attention heads from standard causal attention to calculate the runway-coefficients and can be seamlessly added on top of the standard attention block. To the best of our knowledge, this represents the first solution wherein the attention mechanism is explicitly made into a function of indirect information propagation patterns along the causal graph. For more information on implementation details and precise accounting of parameter counts, refer to Section B.

5. Experiments and Results

We train two decoder-only transformers with multi-head attention: (1) standard transformer for baseline comparisons

and (2) our rewired transformer for runway-aware modeling. Unless specifically stated otherwise, we use the dot-product formulation from Equation (9) for our rewired model which introduces no additional parameters on top of the standard transformer. We use the C4 dataset (Raffel et al., 2020) and train them for next-token prediction. We train models of various sizes, from 50 million parameters up to 750 million parameters, all trained on 20 billion tokens using a global batch size of 256. Unless stated otherwise, context window of 1024 is used as the sequence length. We use Pre-LN (Xiong et al., 2020) instead of Post-LN and use rotary positional encodings (RoPE) (Su et al., 2024). We use the Adam optimizer (Kingma, 2014) and all models are trained on NVIDIA A100 GPUs. For modeling and implementation details, refer to Section B.

5.1. General Language Modeling

Validation Performance. The main language modeling performance comparisons between standard and our rewired transformers are shown in Figure 2. On the left, Figure 2a compares their validation perplexity at varying context window sizes for in-context evaluation. Both standard and rewired transformers are trained with 4 different context window sizes (From 512 to 2048) with 100 million parameters and evaluated at their corresponding train-time context window size. We observe that the rewired transformer outperforms the standard transformer, with its improvements growing with context window size. With growing context window size, so too grows the available runway lengths and thus it is reasonable to expect that our rewired model should show growing improvements compared to standard transformer. On the right, Figure 2b compares validation perplexity for both models at various model sizes, from 50 million to 750 million parameters. The context window size is fixed at 1024. Here we observe modest but consistent performance improvements for our rewired transformer likely stemming from our runway-aware rewiring reducing noise and redundancy accumulation and thus keeping token representations slightly sharper.

Reasoning Benchmarks. We compare our rewired model against standard transformer on reasoning benchmarks using 750 million parameter models in Table 1. For more information on the experimental setup and benchmark datasets used, refer to Section C.1. Overall, we generally observe modest but consistent improvements across benchmarks for our rewired model (best result for each dataset marked in blue). For ARC variants specifically, ARC-Easy focuses on information co-occurrence which may explain our rewired model’s inferior performance as it may over-suppress perceived redundancies in the text. On the other hand, ARC-challenge focuses on multi-hop reasoning and we can see that our rewired model shows a clear advantage compared

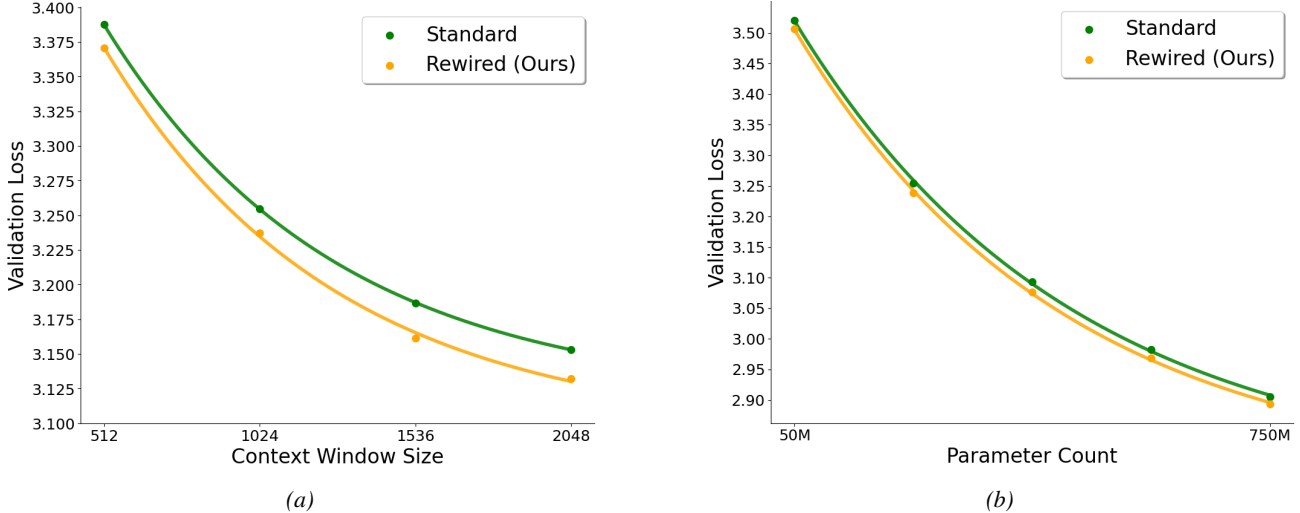


Figure 2. Validation perplexity on the C4 dataset with (a) varying context window sizes (from 512 to 2048) using a 100 million parameter model and (b) varying model sizes from 50 million to 750 million parameters.

to standard transformer in this setting.

Table 1. Reasoning performance of standard and our rewired transformers. Best result from each dataset is marked in blue.

| Dataset | Std. Transformer | Rewired (Ours) |
|----------------|------------------|----------------|
| ARC-Easy | 43.81% | 42.89% |
| ARC-Challenge | 24.66% | 26.11% |
| HellaSwag | 41.75% | 42.49% |
| PIQA | 68.61% | 68.82% |
| CommonsSenseQA | 19.49% | 19.57% |

5.2. Information Retrieval Analysis

We perform passkey retrieval analysis to compare copying and information retrieval abilities of our rewired transformer against the baseline standard transformer. For both standard and rewired transformers, we use 450 million parameter models trained with general language modeling using 1024 as the sequence length from Section 5.1. For this task, a random 5-digit passkey is embedded into the sequence of natural language where the objective is to retrieve the passkey. We only count exact matches and thus all and only the correct 5 digits of the passkey must be retrieved for it to count as successful retrieval. For more information on the experimental setup, refer to Section C.2.

For the main retrieval analysis in Figure 3, we compare performance of both models at varying context window sizes, starting in-context at 1024 and increasing the context window size up to 1536. Passkeys are embedded at 10 different depths for each context length and each context length's performance is run 10 times. Their overall results are averaged and the light shaded regions represent their standard deviation.

As shown in Figure 3, we find that our rewired transformer shows superior retrieval performance compared to the standard transformer. Furthermore, we observe that our rewired version maintains performance for longer while standard transformer's performance collapses much more quickly when taken out of in-context regime. Notably, at context window length of 1280, the standard transformer already shows less than 20% accuracy while our rewired version maintains reasonable performance at above 60%. In fact, the rewired transformer's performance at context length 1280 is comparable to the standard transformer's performance at context length 1216.

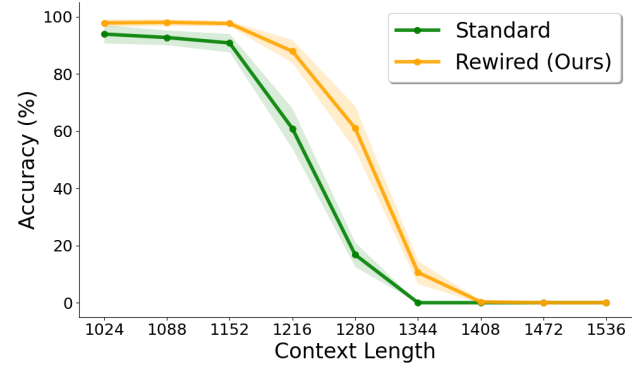


Figure 3. Passkey retrieval test for standard and our rewired transformers. We use 450 million parameter models trained on general language tasks at context length of 1024 and test their retrieval abilities up to context length of 1536.

The superior performance of our rewired transformer beyond the training context length is evidence that runway awareness may contribute to improved long-range information routing. This also shows that our model may be less

sensitive to standard transformers’ failure mode where indirect, multi-hop influences progressively accumulate and overwhelm the intended signal.

Next, we perform depth-based comparisons in Figure 4. The same models from Figure 3 now have their accuracies measured at various depths of passkey placement within the sequence with the sequence length fixed at 1216. Performance at each depth is measured 10 times and averaged with the shaded regions showing the standard deviation.

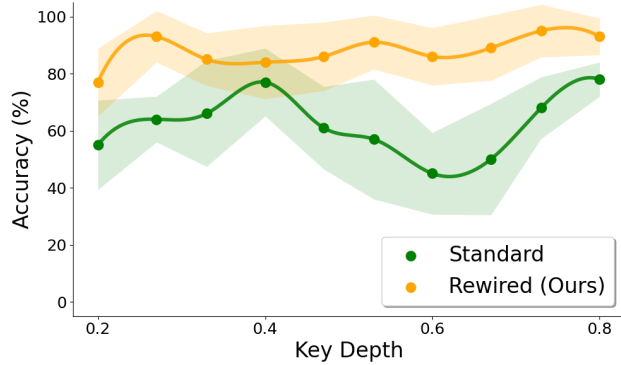


Figure 4. Zero-shot passkey retrieval test for standard and our rewired transformers where passkeys are embedded at varying depths.

Not only do we observe superior performance for the rewired model at every depth, but we also see that the U-shaped curve from lost-in-the-middle effect is completely remedied in the rewired version. In contrast, standard transformer clearly exhibits the U-shaped curve in its performance and shows degradation towards the middle of the sequence, matching observations from prior works (Liu et al., 2024; Barbero et al., 2024). Overall, superior retrieval results despite identical parameter counts suggest that our rewired transformer is better at maintaining representation sharpness and token-level distinctness as the context grows, rather than letting tokens get indistinguishably mixed along the indirect pathways.

5.3. Extrapolation Analysis

Beyond retrieval tasks, we isolate the extrapolation setting to further analyze long-range information routing capabilities of our rewired model compared to standard transformer.

In Figure 5, we show extrapolation abilities of both standard and rewired transformers at sequence length of 2048 across various model sizes. Both models were trained with in-context sequence length of 1024. We observe consistent improvements for our rewired transformer. In addition, we find that standard transformers need around 150 million more parameters to reach comparable extrapolation performance as our rewired model (refer to Section C.3). This parameter efficiency gains suggest that runway-aware

rewiring addresses a fundamental architectural bottleneck of standard attention. As extrapolated contexts create longer runways with more intermediate tokens between source and destination pairs, the progressive accumulation of runway influences may grow more severe, requiring standard transformers to compensate through increased model capacity. In contrast, our rewiring mechanism maintains awareness of runway accumulations by design. The consistent improvements across model size further indicate that our rewiring method is tackling a fundamental architectural limitation of standard transformers, rather than artifacts of insufficient model capacity.

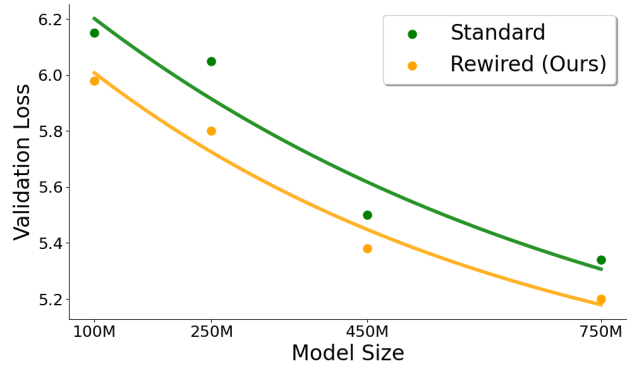


Figure 5. Extrapolation at sequence length 2048 across model sizes for standard and rewired transformers.

5.4. Ablations and Analysis

We provide ablation studies, namely comparing the dot-product rewiring approach with the bilinear form, in Section C.4. We find that they are comparable in performance across tasks. In addition, we examine the attention map and rewiring patterns for our rewired model in Section D. We find that while early tokens are generally down-scaled more heavily than later tokens, the rewiring mechanism learns complex patterns beyond simple distance-based decay and in fact learns to show diverse rewiring behaviors.

6. Conclusion

In this paper, we introduced runway cascade in transformers as the misalignment between direct-path attention and compounding influence of indirect paths along the causal graph. We performed theoretical analysis to examine information propagation patterns in decoder-only transformers and showed how certain redundancies and irrelevant information can cascade forward, invariant to attention mechanism. Building on these theoretical observations, we introduced runway-aware rewiring to better align the attention mechanism with runway influences. Empirically, our rewiring approach showed superior modeling capabilities compared to standard transformers across language tasks.

Impact Statement

This paper presents work whose goal is to advance the field of Machine Learning, specifically in language modeling. There are many potential societal consequences of our work, none which we feel must be specifically highlighted here.

References

Abboud, R., Dimitrov, R., and Ceylan, I. I. Shortest path networks for graph property prediction. In *Learning on graphs conference*, pp. 5–1. PMLR, 2022.

Achiam, J., Adler, S., Agarwal, S., Ahmad, L., Akkaya, I., Aleman, F. L., Almeida, D., Altenschmidt, J., Altman, S., Anadkat, S., et al. Gpt-4 technical report. *arXiv preprint arXiv:2303.08774*, 2023.

Alon, U. and Yahav, E. On the bottleneck of graph neural networks and its practical implications. In *International Conference on Learning Representations*, 2021. URL <https://openreview.net/forum?id=i80OPhOCVH2>.

Arroyo, Á., Barbero, F., Blayney, H., Bronstein, M., Dong, X., Liò, P., Pascanu, R., and Vandergheynst, P. Bridging graph neural networks and large language models: A survey and unified perspective. 2025.

Barbero, F., Banino, A., Kapturowski, S., Kumaran, D., Madeira Araújo, J., Vitvitskyi, O., Pascanu, R., and Veličković, P. Transformers need glasses! information over-squashing in language tasks. *Advances in Neural Information Processing Systems*, 37:98111–98142, 2024.

Barbero, F., Arroyo, A., Gu, X., Perivolaropoulos, C., Veličković, P., Pascanu, R., and Bronstein, M. M. Why do LLMs attend to the first token? In *Second Conference on Language Modeling*, 2025a. URL <https://openreview.net/forum?id=tu4dFUsW5z>.

Barbero, F., Vitvitskyi, A., Perivolaropoulos, C., Pascanu, R., and Veličković, P. Round and round we go! what makes rotary positional encodings useful? In *The Thirteenth International Conference on Learning Representations*, 2025b. URL <https://openreview.net/forum?id=GtvuNrk58a>.

Beltagy, I., Peters, M. E., and Cohan, A. Longformer: The long-document transformer. *arXiv preprint arXiv:2004.05150*, 2020.

Bisk, Y., Zellers, R., Gao, J., Choi, Y., et al. Piqa: Reasoning about physical commonsense in natural language. In *Proceedings of the AAAI conference on artificial intelligence*, volume 34, pp. 7432–7439, 2020.

Black, M., Wan, Z., Nayyeri, A., and Wang, Y. Understanding oversquashing in gnn through the lens of effective resistance. In *International Conference on Machine Learning*, pp. 2528–2547. PMLR, 2023.

Brüel-Gabrielsson, R., Yurochkin, M., and Solomon, J. Rewiring with positional encodings for graph neural networks. *arXiv preprint arXiv:2201.12674*, 2022.

Clark, P., Cowhey, I., Etzioni, O., Khot, T., Sabharwal, A., Schoenick, C., and Tafjord, O. Think you have solved question answering? try arc, the ai2 reasoning challenge. *arXiv preprint arXiv:1803.05457*, 2018.

Comanici, G., Bieber, E., Schaekermann, M., Pasupat, I., Sachdeva, N., Dhillon, I., Blistein, M., Ram, O., Zhang, D., Rosen, E., et al. Gemini 2.5: Pushing the frontier with advanced reasoning, multimodality, long context, and next generation agentic capabilities. *arXiv preprint arXiv:2507.06261*, 2025.

Deac, A., Lackenby, M., and Veličković, P. Expander graph propagation. In *Learning on Graphs Conference*, pp. 38–1. PMLR, 2022.

Di Giovanni, F., Giusti, L., Barbero, F., Luise, G., Lio, P., and Bronstein, M. M. On over-squashing in message passing neural networks: The impact of width, depth, and topology. In *International conference on machine learning*, pp. 7865–7885. PMLR, 2023.

Esser, P., Kulal, S., Blattmann, A., Entezari, R., Müller, J., Saini, H., Levi, Y., Lorenz, D., Sauer, A., Boesel, F., et al. Scaling rectified flow transformers for high-resolution image synthesis. In *Forty-first international conference on machine learning*, 2024.

Fang, L., Wang, Y., Gatmiry, K., Fang, L., and Wang, Y. Rethinking invariance in in-context learning. In *The Thirteenth International Conference on Learning Representations*, 2025. URL <https://openreview.net/forum?id=q1UyoY3MgJ>.

Giovanni, F. D., Rusch, T. K., Bronstein, M., Deac, A., Lackenby, M., Mishra, S., and Veličković, P. How does over-squashing affect the power of GNNs? *Transactions on Machine Learning Research*, 2024. ISSN 2835-8856. URL <https://openreview.net/forum?id=KJRQvRWNs>.

Gu, X., Pang, T., Du, C., Liu, Q., Zhang, F., Du, C., Wang, Y., and Lin, M. When attention sink emerges in language models: An empirical view. In *The Thirteenth International Conference on Learning Representations*, 2025. URL <https://openreview.net/forum?id=78Nn4QJTN>.

Hou, Y., Zhang, J., Lin, Z., Lu, H., Xie, R., McAuley, J., and Zhao, W. X. Large language models are zero-shot rankers for recommender systems. In *European Conference on Information Retrieval*, pp. 364–381. Springer, 2024.

Jamadandi, A., Rubio-Madrigal, C., and Burkholz, R. Spectral graph pruning against over-squashing and over-smoothing. *Advances in Neural Information Processing Systems*, 37:10348–10379, 2024.

Joshi, C. K. Transformers are graph neural networks. *arXiv preprint arXiv:2506.22084*, 2025.

Karhadkar, K., Banerjee, P. K., and Montufar, G. FoSR: First-order spectral rewiring for addressing oversquashing in GNNs. In *The Eleventh International Conference on Learning Representations*, 2023. URL <https://openreview.net/forum?id=3YjQfCLdrzz>.

Kazemnejad, A., Padhi, I., Natesan, K., Das, P., and Reddy, S. The impact of positional encoding on length generalization in transformers. In *Thirty-seventh Conference on Neural Information Processing Systems*, 2023. URL <https://openreview.net/forum?id=Drrl2gcjzl>.

Kingma, D. P. Adam: A method for stochastic optimization. *arXiv preprint arXiv:1412.6980*, 2014.

Liu, N. F., Lin, K., Hewitt, J., Paranjape, A., Bevilacqua, M., Petroni, F., and Liang, P. Lost in the middle: How language models use long contexts. *Transactions of the Association for Computational Linguistics*, 12:157–173, 2024.

Lu, Y., Bartolo, M., Moore, A., Riedel, S., and Stenetorp, P. Fantastically ordered prompts and where to find them: Overcoming few-shot prompt order sensitivity. In *Proceedings of the 60th Annual Meeting of the Association for Computational Linguistics (Volume 1: Long Papers)*, pp. 8086–8098, 2022.

Raffel, C., Shazeer, N., Roberts, A., Lee, K., Narang, S., Matena, M., Zhou, Y., Li, W., and Liu, P. J. Exploring the limits of transfer learning with a unified text-to-text transformer. *Journal of machine learning research*, 21(140):1–67, 2020.

Shirzad, H., Velingker, A., Venkatachalam, B., Sutherland, D. J., and Sinop, A. K. Exphormer: Sparse transformers for graphs. In *International Conference on Machine Learning*, pp. 31613–31632. PMLR, 2023.

Shirzad, H., Lin, H., Venkatachalam, B., Velingker, A., Woodruff, D., and Sutherland, D. J. Even sparser graph transformers. In *The Thirty-eighth Annual Conference on Neural Information Processing Systems*, 2024. URL <https://openreview.net/forum?id=K3k4bWuNnk>.

Speer, R., Chin, J., and Havasi, C. Conceptnet 5.5: An open multilingual graph of general knowledge. In *Proceedings of the AAAI conference on artificial intelligence*, volume 31, 2017.

Sterner, I., Su, S., and Veličković, P. Commute-time-optimised graphs for gnns. *arXiv preprint arXiv:2407.08762*, 2024.

Su, J., Ahmed, M., Lu, Y., Pan, S., Bo, W., and Liu, Y. Roformer: Enhanced transformer with rotary position embedding. *Neurocomputing*, 568:127063, 2024.

Talmor, A., Herzig, J., Lourie, N., and Berant, J. Commonsenseqa: A question answering challenge targeting commonsense knowledge. In *Proceedings of the 2019 Conference of the North American Chapter of the Association for Computational Linguistics: Human Language Technologies, Volume 1 (Long and Short Papers)*, pp. 4149–4158, 2019.

Topping, J., Giovanni, F. D., Chamberlain, B. P., Dong, X., and Bronstein, M. M. Understanding over-squashing and bottlenecks on graphs via curvature. In *International Conference on Learning Representations*, 2022. URL <https://openreview.net/forum?id=7UmjRGzp-A>.

Wilson, J., Bechler-Speicher, M., and Veličković, P. Cayley graph propagation. In *The Third Learning on Graphs Conference*, 2024. URL <https://openreview.net/forum?id=VaTfEDs61E>.

Wu, X., Ajorlou, A., Wu, Z., and Jadbabaie, A. Demystifying oversmoothing in attention-based graph neural networks. *Advances in Neural Information Processing Systems*, 36:35084–35106, 2023.

Wu, X., Ajorlou, A., Wang, Y., Jegelka, S., and Jadbabaie, A. On the role of attention masks and layernorm in transformers. *Advances in Neural Information Processing Systems*, 37:14774–14809, 2024.

Wu, X., Wang, Y., Jegelka, S., and Jadbabaie, A. On the emergence of position bias in transformers. In *Forty-second International Conference on Machine Learning*, 2025. URL <https://openreview.net/forum?id=YufVkJ6IIi>.

Xiao, G., Tian, Y., Chen, B., Han, S., and Lewis, M. Efficient streaming language models with attention sinks. In *The Twelfth International Conference on Learning Representations*, 2024. URL <https://openreview.net/forum?id=NG7sS51zVF>.

Xiong, R., Yang, Y., He, D., Zheng, K., Zheng, S., Xing, C., Zhang, H., Lan, Y., Wang, L., and Liu, T. On layer

normalization in the transformer architecture. In *International conference on machine learning*, pp. 10524–10533. PMLR, 2020.

Zaheer, M., Guruganesh, G., Dubey, K. A., Ainslie, J., Alberti, C., Ontanon, S., Pham, P., Ravula, A., Wang, Q., Yang, L., et al. Big bird: Transformers for longer sequences. *Advances in neural information processing systems*, 33:17283–17297, 2020.

Zellers, R., Holtzman, A., Bisk, Y., Farhadi, A., and Choi, Y. Hellaswag: Can a machine really finish your sentence? *arXiv preprint arXiv:1905.07830*, 2019.

A. Proofs

A.1. Token Sensitivity Analysis

In order to draw sensitivity bounds on causal transformers in terms of the relative runway of the given token pair, it needs to account for arbitrary tokens and arbitrary layers. However, most over-squashing bounds in GNN literature only bound the Jacobian of a node at the final layer with respect to a node at the input layer. In addition, most works also assume a fixed, binary graph structure, which can simply be expressed as a power of the number of layers in the Jacobian bound. However, since transformers employ dynamic attention patterns in each layer, the fixed topology bound does not apply directly. As such, we draw a general over-squashing bound using the Jacobian of arbitrary nodes h_d, h_s at arbitrary layers $L+r$ and L , for $L \geq 0$ and $r \geq 0$. This is formulated below with Theorem A.1 which incorporates over-squashing bounds for any two nodes at any two layers and accounting for dynamic attention patterns in each layer. In our proofs, we make the simplifying assumption that attention weights are independent of h , following the convention of (Barbero et al., 2024). Likewise, we also assume supplementary operations such as layer-norms and residual connections are absorbed into ϕ and bounded. We use these simplifying assumptions to draw clean bounds highlighting information propagation patterns for interpretive purposes. In reality, the attention weights would be a function of token representations but their corresponding information propagation patterns from a topological point-of-view would remain unchanged from our analysis.

Theorem A.1. *Assume a token h_s at layer $L \geq 0$ and another token h_d at $r \geq 0$ layers apart and on arbitrary positions $s \leq d$. In addition, let $C > 0$ be some constant and A be lower-triangular, row-stochastic adjacency operator. Then, the representational sensitivity of h_d with respect to h_s can be bounded as:*

$$\left\| \frac{\partial h_d^{(L+r)}}{\partial h_s^{(L)}} \right\| \leq C^r \left(\prod_{t=0}^{r-1} (I + A^{(L+t)}) \right)_{ds}$$

Proof. We prove this by induction on layer r . For the base case of $r = 0$, either $d = s$ or $d \neq s$, and thus

$$\frac{\partial h_d^{(L)}}{\partial h_s^{(L)}} = \begin{cases} I & \text{if } d = s, \\ 0 & \text{if } d \neq s, \end{cases}$$

where I is the (feature-dimension) identity matrix and 0 is the zero matrix. Therefore,

$$\left\| \frac{\partial h_d^{(L)}}{\partial h_s^{(L)}} \right\| = \begin{cases} I & \text{if } d = s, \\ 0 & \text{if } d \neq s, \end{cases} = \delta_{ds} \leq (I)_{ds}.$$

Assume that the statement holds for some $r \geq 0$. We now prove the case for layer $r+1$ by induction.

$$\begin{aligned} \left\| \frac{\partial h_d^{(L+r+1)}}{\partial h_s^{(L)}} \right\| &= \left\| \partial_1 \phi_{L+r} \cdot \frac{\partial h_d^{(L+r)}}{\partial h_s^{(L)}} + \partial_2 \phi_{L+r} \sum_{w \in \mathcal{N}_d} A_{dw}^{(L+r)} \partial \psi_{L+r} \cdot \frac{\partial h_w^{(L+r)}}{\partial h_s^{(L)}} \right\| \\ &\leq \|\partial_1 \phi_{L+r}\| \cdot \left\| \frac{\partial h_d^{(L+r)}}{\partial h_s^{(L)}} \right\| + \|\partial_2 \phi_{L+r}\| \cdot \|\partial \psi_{L+r}\| \cdot \sum_{w \in \mathcal{N}_d} A_{dw}^{(L+r)} \cdot \left\| \frac{\partial h_w^{(L+r)}}{\partial h_s^{(L)}} \right\| \end{aligned}$$

Let $C \geq \|\nabla \phi\|$ and $C \geq \|\nabla \phi\| \cdot \|\nabla \psi\|$,

$$\begin{aligned} &\leq C \cdot \left\| \frac{\partial h_d^{(L+r)}}{\partial h_s^{(L)}} \right\| + C \cdot \sum_{w \in \mathcal{N}_d} A_{dw}^{(L+r)} \cdot \left\| \frac{\partial h_w^{(L+r)}}{\partial h_s^{(L)}} \right\| \\ &\leq C C^r \left(\prod_{t=0}^{r-1} (I + A^{(L+t)}) \right)_{ds} + C \sum_{w \in \mathcal{N}(d)} A_{dw}^{(L+r)} C^r \left(\prod_{t=0}^{r-1} (I + A^{(L+t)}) \right)_{ws} \quad (\text{induction}) \\ &= C^{r+1} \left(\left(\prod_{t=0}^{r-1} (I + A^{(L+t)}) \right)_{ds} + \sum_{w \in \mathcal{N}(d)} A_{dw}^{(L+r)} \left(\prod_{t=0}^{r-1} (I + A^{(L+t)}) \right)_{ws} \right) \end{aligned}$$

Defining $A_{dw}^{(l)} = 0$ for $w \notin \mathcal{N}(d)$

$$\begin{aligned}
 &= C^{r+1} \left((I + A^{(L+r)}) \prod_{t=0}^{r-1} (I + A^{(L+t)}) \right)_{ds} && \text{(definition of matrix multiplication)} \\
 &= C^{r+1} \left(\prod_{t=0}^r (I + A^{(L+t)}) \right)_{ds}
 \end{aligned}$$

Therefore,

$$\left\| \frac{\partial h_d^{(L+r+1)}}{\partial h_s^{(L)}} \right\| \leq C^{r+1} \left(\prod_{t=0}^r (I + A^{(L+t)}) \right)_{ds}$$

This concludes the proof for Theorem A.1. \square

A.2. Blindspots for Softmax Attention and Runway Cascade

In order to construct our theoretical results on blindspots for attention mechanism, we first quickly review the translation invariance property of the softmax function.

Lemma A.2 (Translation invariance of softmax). *SoftMax_j(z_i) = SoftMax_j($z_i + F$) where F denotes some common factor for all z_i , $i \in \mathcal{N}(j)$*

Proof.

$$\begin{aligned}
 \text{SoftMax}_j(z_i + F) &= \frac{e^{(z_i + F)}}{\sum_j e^{(z_j + F)}} \\
 &= \frac{e^F e^{z_i}}{\sum_j e^F e^{z_j}} = \frac{e^F e^{z_i}}{e^F \sum_j e^{z_j}} \\
 &= \frac{e^{z_i}}{\sum_j e^{z_j}}
 \end{aligned}$$

Therefore, $\text{SoftMax}_j(z_i + F) = \text{SoftMax}_j(z_i)$.

This concludes the proof for Lemma A.2. \square

Lemma A.3 (Blindspots for standard attention mechanism). *Let token representation $h_w = \tilde{h}_w + \delta$ where \tilde{h}_w is (unique) token representation that differentiates h_w and δ denotes the runway influences on h_w . Assume also that δ can be further decomposed into $\delta = \delta_c + \delta_r$ where δ_c is the row-wise perturbation (common mode influence) and δ_r is the residual deviation from row-wise perturbation. Then, attention weights cannot discern runway influences except through (small) residual deviations as:*

$$\|a_d - \tilde{a}_d\| \leq \sigma_0 P \|\delta_r\|$$

Proof.

We use σ to denote the softmax function here.

$$a_{dw} = \sigma_{\mathcal{N}(d)} \left(\frac{h_d W_Q (h_w W_K)^T}{\sqrt{d}} \right) = \sigma_{\mathcal{N}(d)} \left(\frac{h_d W_Q ((\tilde{h}_w + \delta_c + \delta_r) W_K)^T}{\sqrt{d}} \right), \quad \forall w \in \mathcal{N}(d)$$

Expanding the numerator $n = h_d W_Q((\tilde{h}_w + \delta_c + \delta_r)W_K)^T$,

$$\begin{aligned} n &= h_d W_Q(\tilde{h}_w W_K + \delta_c W_K + \delta_r W_K)^T \\ &= h_d W_Q(\delta_c W_K)^T + h_d W_Q(\tilde{h}_w W_K + \delta_r W_K)^T \end{aligned} \quad (\text{factoring})$$

plugging n back into softmax logit numerator,

$$a_{dw} = \sigma_{\mathcal{N}(d)} \left(\frac{h_d W_Q(\delta_c W_K)^T + h_d W_Q(\tilde{h}_w W_K + \delta_r W_K)^T}{\sqrt{d}} \right)$$

Taking $F_{\text{common}} = \frac{h_d W_Q(\delta_c W_K)^T}{\sqrt{d}}$ for all keys $h_w W_K$, $\forall w \in \mathcal{N}(d)$,

$$a_{dw} = \sigma_{\mathcal{N}(d)} \left(F_{\text{common}} + \frac{h_d W_Q(\tilde{h}_w W_K + \delta_r W_K)^T}{\sqrt{d}} \right) = \sigma_{\mathcal{N}(d)} \left(\frac{h_d W_Q(\tilde{h}_w W_K + \delta_r W_K)^T}{\sqrt{d}} \right) \quad (\text{translation invariance Lemma A.2})$$

Then the Lipschitz bound between a_d and \tilde{a}_d can be formulated as:

$$\|a_d - \tilde{a}_d\| \leq \sigma_0 P \|\delta_r\| \quad (15)$$

where σ_0 is the global Lipschitz constant and P is the bound on model terms for h_d 's direct-path attention defined as: $P = \frac{\|h_d W_Q\| \|W_K\|}{\sqrt{d}}$

Therefore,

$$\|a_d - \tilde{a}_d\| \leq \sigma_0 P \|\delta_r\|$$

This concludes the proof for Lemma A.3. \square

Theorem A.4 (Runway Cascade). *Let token representation $h_w = \tilde{h}_w + \delta$ where \tilde{h}_w is (unique) token representation that differentiates h_w and δ denotes the runway influences on h_w . Assume also that δ can be further decomposed into $\delta = \delta_c + \delta_r$ where δ_c is the row-wise perturbation (common mode influence) and δ_r is the residual deviation from row-wise perturbation. Then, their common mode runway influence must persist and cascade forward in the attention mechanism.*

Proof.

Let the attention-aggregated message be $m_d = \sum_{w \in \mathcal{N}(d)} a_{dw} h_w W_V$ where $a_{dw} = \text{SoftMax}_{\mathcal{N}(d)} \left(\frac{h_d W_Q \cdot (h_w W_K)^T}{\sqrt{d}} \right)$. We have established in Lemma A.3 that each a_{dw} is blind to common mode influences.

$$\begin{aligned} m_d &= \sum_{w \in \mathcal{N}(d)} a_{dw} h_w W_V = \sum_{w \in \mathcal{N}(d)} a_{dw} (\tilde{h}_w + \delta_c + \delta_r) W_V \\ &= \sum_{w \in \mathcal{N}(d)} a_{dw} \tilde{h}_w W_V + a_{dw} \delta_c W_V + a_{dw} \delta_r W_V \\ &= \sum_{w \in \mathcal{N}(d)} a_{dw} \delta_c W_V + \sum_{w \in \mathcal{N}(d)} (a_{dw} \tilde{h}_w W_V + a_{dw} \delta_r W_V) \end{aligned}$$

Leveraging row-stochasticity of causal attention weights where $\sum_{w \in \mathcal{N}(d)} a_{dw} = 1.0$,

$$= \delta_c W_V + \sum_{w \in \mathcal{N}(d)} a_{dw} (\tilde{h}_w + \delta_r) W_V$$

Therefore,

$$m_d = \delta_c W_V + \sum_{w \in \mathcal{N}(d)} a_{dw} (\tilde{h}_w + \delta_r) W_V$$

This concludes the proof for Theorem A.4. \square

Overall, Lemma A.3 and Theorem A.4 illustrate how common mode runway influences are invariant to the attention mechanism and that these influences can cascade forward, potentially resulting in accumulations of noise and redundancies. The accumulation of common mode influences can be explained by theory of over-smoothing in attention-based aggregation schemes, where attention acts as a contractive mixing operator that drives token representations closer together with repeated application (Wu et al., 2023; Barbero et al., 2025a; Arroyo et al., 2025). While we isolate the attentional component of the transformer to drive our theoretical conclusions, it should be noted that with the application of additional components such as MLPs and layer-norms, things can become less straight-forward. Specifically, layer-norms have been shown to be able to prevent over-smoothing to the point of complete rank collapse (Wu et al., 2024) with the same work also providing counter-examples of when layer-norms cannot prevent over-smoothing.

B. Implementation Details

In this section, we discuss implementation and comparison details for our rewired transformers and baseline standard transformers.

Training Setup. For training, we use the C4 dataset (Raffel et al., 2020) and train them for standard next-token prediction using 20 billion tokens and global batch size of 256. Unless otherwise stated, context window of 1024 is used as the sequence length. We use Pre-LN (Xiong et al., 2020) instead of Post-LN and use rotary positional encodings (RoPE) (Su et al., 2024). We use the Adam optimizer (Kingma, 2014).

Model Parametrization. We train models of various sizes, from 50 million parameters up to 750 million parameters. We follow conventions from (Esser et al., 2024) and set model size with parameter d s.t. $d_{\text{model}} = 64d$ and both number of attention heads and layers correspond to d . The precise parameter counts are shown in Table 2.

Table 2. Model Parameterization.

| $d = n_{\text{heads}} = n_{\text{layers}}$ | d_{model} | Model Parameter Count |
|--|--------------------|-----------------------|
| 8 | 512 | 50,927,104 |
| 12 | 768 | 123,607,296 |
| 16 | 1024 | 252,890,112 |
| 20 | 1280 | 457,726,720 |
| 24 | 1536 | 756,969,984 |

Runway Aware Rewiring Implementation Details. Here we provide implementation details for our runway-aware rewiring methodology. We re-purpose one of the attention heads to calculate runway-coefficients. The attention head is used for regular MHA as usual. We calculate runway-coefficients once from the re-purposed attention head and use them for all attention heads, instead of calculating runway-coefficients independently for each head. While each attention head typically learns different patterns, we find that this setup results in good performance while achieving memory and computational efficiency. We show pseudo-code for implementing attention with runway-aware rewiring in Listing 1.

C. Experimental Details, Ablation Studies, and Additional Results

Here, we provide more details regarding experimental setup as well as some additional results and ablation studies.

C.1. Reasoning Benchmarks

We use 5 reasoning benchmarks to compare performance between standard transformer our rewired transformer. We use the 750 million parameter models trained on standard next-token-prediction task on the C4 dataset and perform zero-shot reasoning on all 6 datasets without finetuning. More information on each benchmark dataset is compiled below.

ARC-Easy/Challenge (Clark et al., 2018). AI2 Reasoning Challenge (ARC) are multiple choice science questions, split into easy and challenging variations. ARC-Easy includes questions answerable by simple information retrieval or information co-occurrence methods. On the other hand, ARC-Challenge consists of questions that cannot simply be answered by either information retrieval or information co-occurrence, stressing multi-hop reasoning capabilities. Inputs are short natural language questions with four answer options, and the evaluation metric is normalized accuracy.

HellaSwag (Zellers et al., 2019). HellaSwag is a large-scale common sense benchmark testing the models’ abilities to choose plausible continuation of multi-sentence contexts. This task stress-tests procedural knowledge (i.e. “what comes next”) in lieu of factual recall. This aspect of HellaSwag distinguishes it from other reasoning benchmarks like the ARC variants and offers evaluation diversity.

PIQA (Bisk et al., 2020). Physical Interaction: Question Answering (PIQA) focuses on physical common sense. Each instance presents a shot goal or description of a physical task and two candidate solutions, and the model must select the physically more plausible option. These scenarios target physical actions like intuitive physics and object usage, so success depends on grounded world knowledge rather than purely linguistic pattern recognition.

CommonSenseQA (Talmor et al., 2019). CommonSenseQA comprises of five-choice questions generated by sampling ConceptNet (Speer et al., 2017) and asking annotators to write questions whose correct answer is the target concept while distractors are other semantically related concepts. The resulting questions emphasize everyday common sense relations such as causes, purposes, locations, and attributes, testing model ability to use structured common sense rather than shallow linguistic pattern recognition.

C.2. Information Retrieval Analysis.

We perform zero-shot passkey retrieval on models trained on next-token prediction with sequence length of 1024. Starting in-context at sequence length of 1024, we increase the sequence lengths out-of-context to observe performance degradation and failure points of both standard and our rewired transformers. The needle and retrieval prompt are as follows:

Needle: “The passkey is [passkey #].”

Retrieval Prompt: “The passkey is”

where [passkey #] is a random 5-digit passkey to be retrieved. The objective is to correctly output the embedded passkey in the next-token prediction following the retrieval prompt. As mentioned, we count exact matches only, so all 5 digits and only the correct digits in the right order must be retrieved. This puts emphasis on representation sharpness and fidelity by design. The needle is placed at designated sequence depth (where lower depth means closer to the beginning of sequence) and the rest of the sequence is populated with natural language from the C4 dataset.

C.3. Extrapolation Analysis.

We perform extrapolation on models trained on next-token prediction with sequence length of 1024, same as the retrieval analysis. Starting in-context at 1024, we increase the sequence lengths up to 2048 and observe standard evaluation loss and extrapolation abilities of both standard and our rewired transformers.

In Figure 6a, we compare the extrapolation abilities of our rewired transformer at 100 million parameters and 250 million parameters against the standard transformer at 250 million parameters. Notably, our rewired transformer at 100 million parameters show better extrapolation performance compared to the standard transformer at 250 million parameters. We

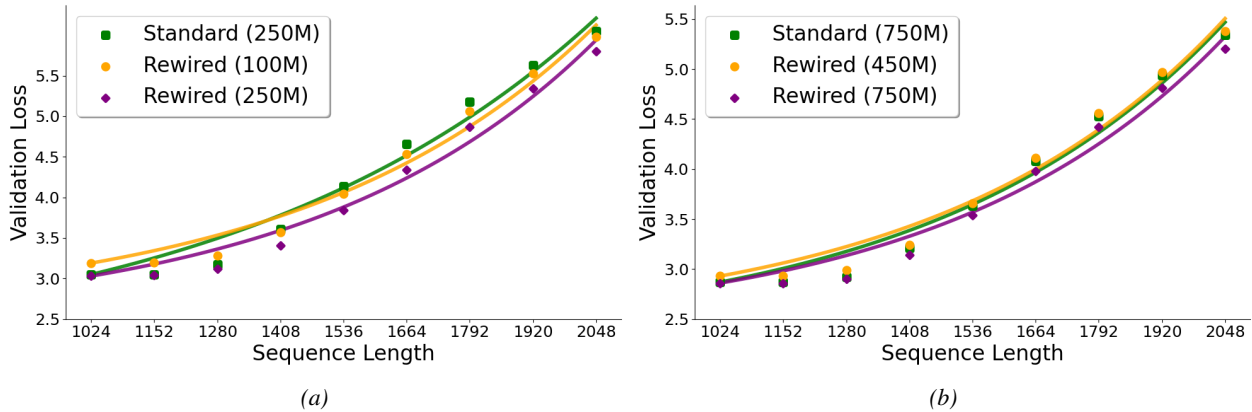


Figure 6. Analysis of extrapolation performance (validation perplexity). Notably, we find that our rewired models show comparable extrapolation performance to standard transformers with 150 million additional parameters.

observe similar results in Figure 6b comparing standard transformer at 750 million parameters against our rewired transformer at 450 million. Overall, Figure 6 shows that standard transformers need around 150 million additional parameters to match our rewired transformers’ extrapolation performance and that this persists at different model scales. Intuitively, our runway-aware rewiring can help extrapolation because longer-than-trained contexts create longer runways, so a method that rewrites and mitigates progressive runway influences should degrade more gracefully as context length increases.

Next, we show additional results in Figure 7, showing extrapolation comparisons across 4 model sizes (100, 250, 450, and 750 million parameters). As illustrated in Figure 7, we see that our rewired model generally outperforms standard transformer in extrapolation across model sizes, and that the improvements seem to grow with growing model size. Coupled with findings from Section 5.3, this indicates that our rewired transformer learns effective information routing patterns that translate to longer-than-trained context lengths better than standard transformers, and that this behavior scales favorably with model size.

C.4. Ablation Studies

We perform ablation studies on runway coefficient calculation methods. Namely, we compare the parameter-free method of using dot-product (used in our experiments) with the learnable bilinear form. When using the bilinear form, the rewired model introduces additional parameters by design. We show its precise parameter count increase in percentage compared to standard transformer at each model size in Table 3 when using the bilinear form. Note that even when using the bilinear form, the parameter-count increase is negligible compared to standard transformers.

Table 3. Model Parameterization and total parameter difference (in percent increase) between the rewired transformer using bilinear form and standard transformer at each model size.

| Total Parameter Count | | | | |
|-----------------------|--------------------|------------------|-------------------------|--------------------|
| d | d_{model} | Std. Transformer | Rewired (Bilinear Form) | Parameter Δ |
| 8 | 512 | 50,927,104 | 50,959,872 | +0.06% |
| 12 | 768 | 123,607,296 | 123,656,448 | +0.04% |
| 16 | 1024 | 252,890,112 | 252,955,648 | +0.03% |
| 20 | 1280 | 457,726,720 | 457,808,640 | +0.02% |
| 24 | 1536 | 756,969,984 | 757,068,288 | +0.01% |

Figure 8 shows the main ablation comparing validation loss of the bilinear form rewiring (orange circle) versus the dot-product rewiring (purple diamond) methods. Standard transformer performance (green square) is also included for baseline visualization. We see that the bilinear form and dot-product approaches are comparable in performance.

Figure 9 shows sequence length ablation of both rewired models using dot-product (purple diamond) and bilinear form (orange circle) for runway-coefficient calculation. Standard transformer (in green square) is included for baseline visualization.

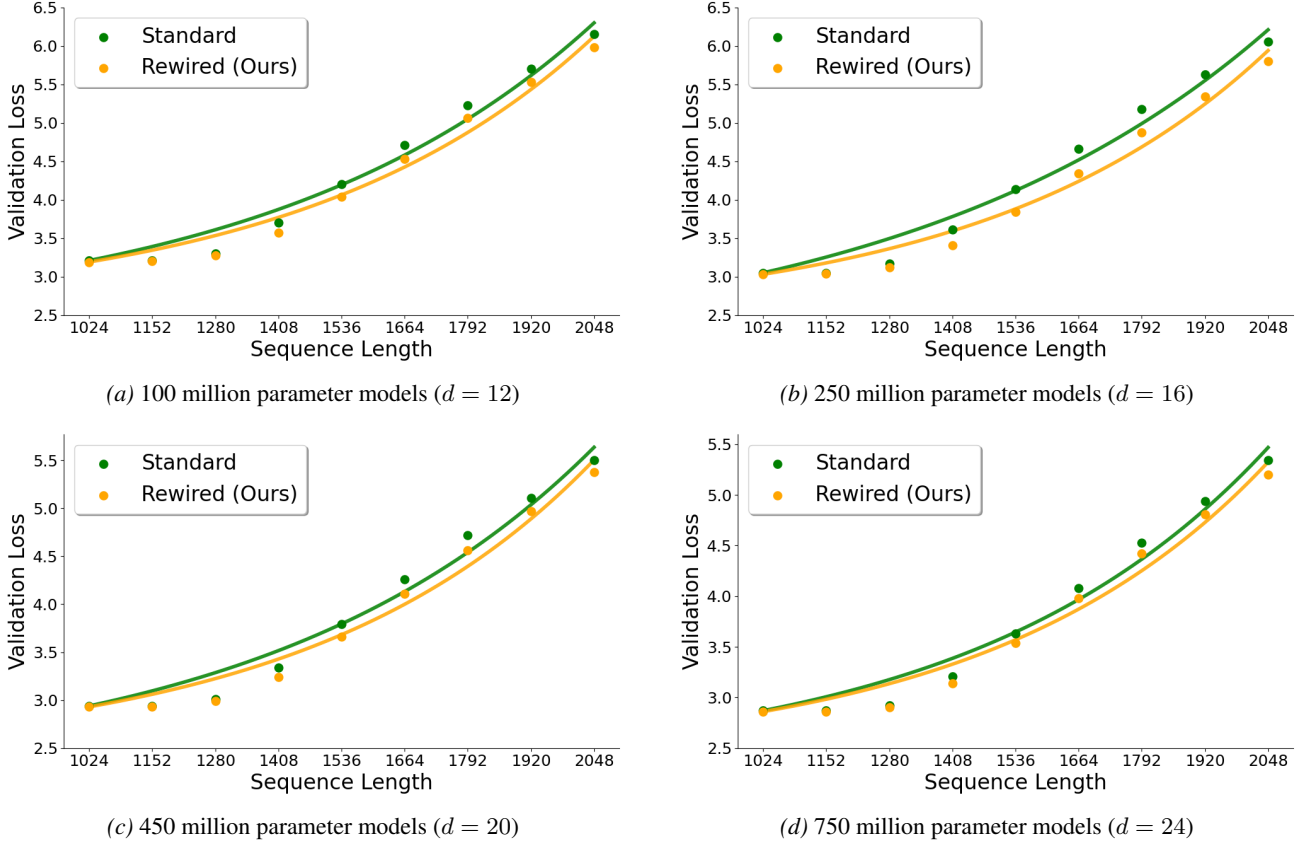


Figure 7. Extrapolation comparison between standard and rewired transformers at various model sizes: (a) 100 million parameters, (b) 250 million parameters, (c) 450 million parameters, and (d) 750 million parameters.

tion. We see that performance between dot-product and bilinear form methods are comparable, showing that our overall runway-aware rewiring learns approximately equally effective rewiring patterns whether we introduce additional parameters or not.

Figure 10 shows extrapolation abilities for transformers with dot-product rewiring compared against bilinear form rewiring. Standard transformer is included for baseline measurements and all models are using 450 million parameters. We see that using dot-product for runway-coefficient calculation is slightly worse than using bilinear form but nonetheless results in superior performance compared to standard transformer. Because this dot-product approach is completely parameter-free, its improvement against standard transformer reinforces the utility of runway-aware rewiring.

D. Rewiring Pattern Analysis

Here we conduct analysis over the rewiring behaviors and the overall attention patterns in our 450 million parameter rewired transformer.

Figure 11 visualizes the strength of \bar{r} in the overall attention map. Purple colors denote stronger down-scaling and thus more aggressive rewiring and white and green colors denote weaker down-scaling. Overall, we see that token pairs with longer runways (near the bottom left corner of the matrix) get down-scaled heavily while tokens with shorter runways (near the diagonal) are relatively unaffected by rewiring. Further more, we see that even though token pairs with longer runways typically see stronger down-scaling, the effect is not necessarily uniform and there are many instances where these pairs avoid strong down-scaling (shown in neutral white colors that form a checkered pattern among the purple regions in the bottom left corner). This shows that our runway-aware rewiring is not learning trivial, generalized patterns such as uniform distance-based decay, but rather it can learn to be flexible and choose complex rewiring patterns.

Figure 12 chart average \bar{r} applied (a) to each source token (Figure 12a) and (b) by each destination token Figure 12b. Lower

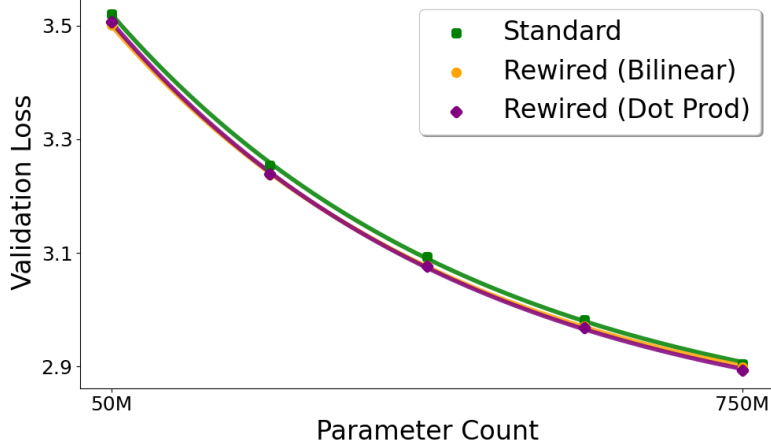


Figure 8. Validation loss comparison at various model sizes between rewired model using dot product (in purple) and bilinear form (in orange). Standard transformer (in green) is included for baseline comparison.

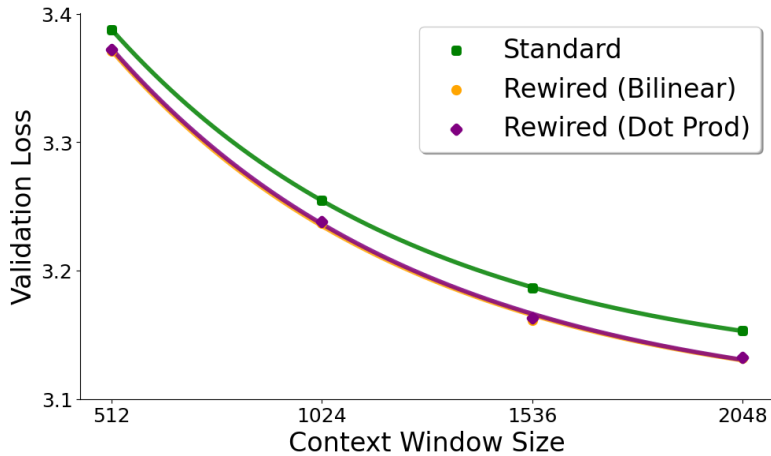


Figure 9. Context window size ablation for rewired transformer with dot product (purple diamond) and bilinear form (orange circle) runway-coefficient calculation. Standard transformer performance (in green square) is also plotted for baseline information.

values indicate stronger down-scaling and thus more aggressive rewiring. The shaded regions illustrate standard deviation and signify diversity of \bar{r} applied to/by each token.

Figure 12a charts the average \bar{r} applied to each source token by all future tokens. As such, we see an increasing trend across source token positions, with early tokens being down-scaled more heavily than later tokens on average. The shaded region is the standard deviation and shows the diversity of \bar{r} applied to each source token. We see that the standard deviations are quite high for the initial two-thirds of source tokens in the sequence, showing that different future tokens apply different scaling factors to them. This again shows that the rewiring mechanism is not simply down-scaling early tokens in a uniform, distance-based decay but is showing more complex patterns where different future tokens apply noticeably different down-scaling for earlier tokens, even though on average, earlier tokens get down-scaled more as expected. The first few source tokens are not down-scaled as a result of our rewiring methodology and thus shows a spike at the very left end of the chart.

Figure 12b charts the average \bar{r} for each destination token's row-wise attention pattern. In other words, this chart represents a horizontal slice through the rewiring pattern matrix, averaging across columns for each row. Thus, this chart shows how much each token down-scales its own attention on average. We see a clean downward pattern across destination token positions, with growing standard deviations. Generally, this means that destination tokens toward the tail-end of the sequence apply stronger and more diverse rewiring, which makes sense given that later tokens have to work with longer runways.

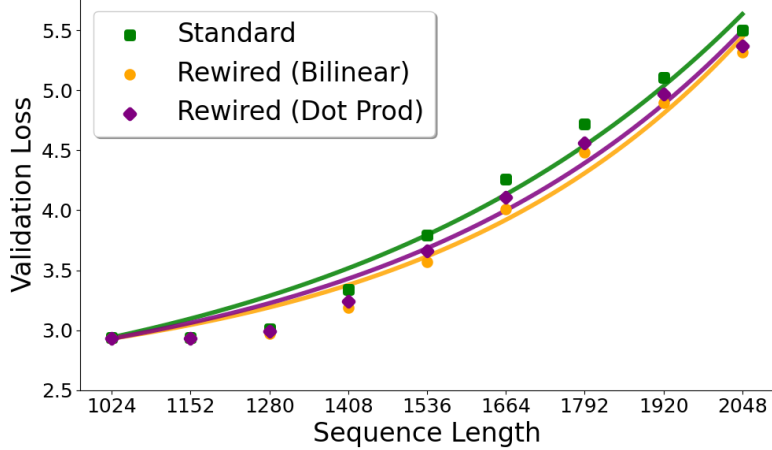


Figure 10. Extrapolation analysis for our rewired transformers using dot product (in purple diamond) and bilinear form (in orange circle). Standard transformer (in green square) is used for baseline visualization. All models are using 450 million parameters.

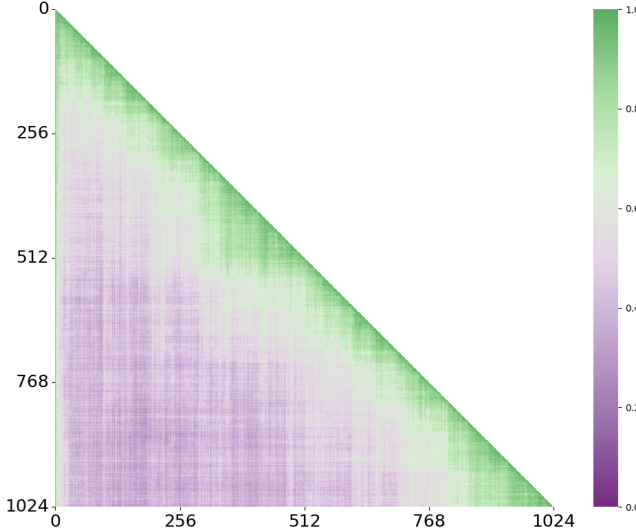


Figure 11. Visualization of the strength of edge down-scaling factor \bar{r} in the overall lower-triangular attention map (averaged over all heads). Lower values (which are more purple) indicate stronger down-scaling and therefore more aggressive rewiring.

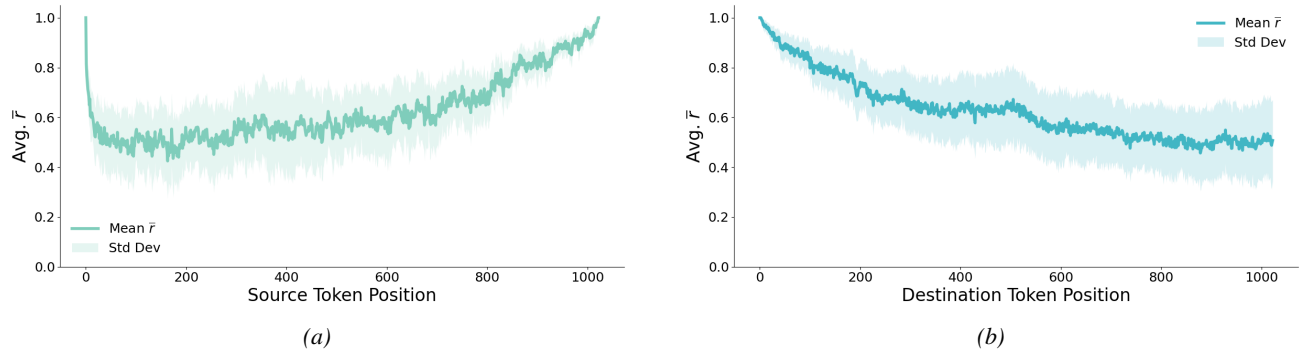


Figure 12. The average down-scaling effect of \bar{r} with respect to each (a) source token position and (b) destination token position.

Listing 1. Attention with Runway Aware Rewiring (Pseudo code)

```

def runway_rewired_attention(x, is_causal=True):
    Q, K, V = project_qkv(x)  # each: [batch, n_heads, seq_len, head_dim]

    Q, K = RoPE(Q, K)

    # standard attention logic
    logits = (Q @ K.T) / sqrt(head_dim)

    i = torch.arange(seq_len).view(1,1,seq_len,1)
    j = torch.arange(seq_len).view(1,1,1,seq_len)

    causal_mask = (j <= i)                                # standard causality
    keep_adjacent = (j == i) | (j == i-1) | (j == 0)      # keep self, prev, first token
    eligible_for_rewiring = (j <= i-2)

    # extract last head to re-purpose for runway coefficients
    V_last = V[:, -1:, :, :]  # [batch, 1, seq_len, head_dim]

    # get V_{i-1} for each position i
    V_prev = V_last[:, :, prev_indices, :]  # [batch, 1, seq_len, head_dim]

    # runway-coefficient calculation
    R_scores = v_prev @ v_last.T
    R_scores = R_scores / sqrt(self.head_dim)

    R = sigmoid(R_scores)  # runway-coefficient in (0, 1)

    beta = 1 - R  # higher beta = lower R

    # Override: always keep adjacent edges (no rewiring)
    beta = where(keep_adjacent, 1.0, beta)

    # Only apply rewiring to eligible edges
    beta = where(eligible_for_rewiring, beta, 1.0)

    # Broadcast to all heads
    beta = beta.expand(batch, n_heads, seq_len, seq_len)

    # standard attention logic
    masked_logits = logits.masked_fill(~causal_mask, -inf)
    attn = softmax(masked_logits, dim=-1)

    # applying rewiring
    attn_rewired = attn * beta

    # re-normalizing attn_rewired to sum up to 1.0 in each row
    attn_rewired = attn_rewired / attn_rewired.sum(dim=-1)

    # standard attention logic
    out = attn_rewired @ V  # [batch, n_heads, seq_len, head_dim]
    out = concat_heads(out)  # [batch, seq_len, d_model]
    out = project_out(out)

return out

```